# Imaging rings in Ring Imaging Cherenkov counters

## Blair N. Ratcliff

*Stanford Linear Accelerator Center, Stanford University, P.O. Box 20450, Stanford, CA 94309, USA*

**Abstract**

The general concepts used to form images in Ring Imaging Cherenkov (RICH) counters are described and their performance properties compared. Particular attention is paid to issues associated with imaging in the time dimension, especially in Detectors of Internally Reflected Cherenkov light (DIRC).
© 2003 Elsevier Science B.V. All rights reserved.

*PACS:* 41.60.Bq; 29.40.Ka

*Keywords:* RICH; DIRC; PID; Cherenkov counters; Ring imaging; Particle identification

## 1. Introduction and scope

The most powerful information available for tracking and particle identification using the Cherenkov process lies in measurements of the ring-correlated angles of emission of the visible and UV Cherenkov photons with respect to the particle trajectory. Since low-energy photon detectors can measure only the detection time and position of an individual photon (not the angles directly), the photons must be 'imaged' onto a detector so that angles can be derived. This paper attempts to clarify some of the issues associated with this imaging process in Ring Imaging Cherenkov (RICH) counters. In an attempt to make the principles involved transparent, much of this discussion is pedagogical in tone and presented at a 'schematic' level. Particular emphasis is placed on the utilization of the timing dimension for high-resolution imaging. Some of these issues have been discussed previously, e.g., at the last

workshop in this series, RICH98 [1], and more completely elsewhere [2] for the particular case of Detectors of Internally Reflected Cherenkov light (DIRC). The author regrets that space limitations do not allow much of the explanatory material presented at the conference to be discussed here.

## 2. Fundamentals

### 2.1. Basic Cherenkov equations

As is well known, Cherenkov radiation is emitted at polar angle ($\theta_c$), uniformly in azimuthal angle ($\varphi_c$), with respect to the particle path

$$\cos \theta_c = \frac{1}{\beta n(\lambda)} \tag{1}$$

where $\beta = v_p/c$. $v_p$ is the particle velocity, $c$ is the speed of light, and $n(\lambda)$ is the index of refraction of the material. Since the index of refraction is a function of the photon wavelength, in normal optical materials there is an 'intrinsic' Cherenkov

---

*E-mail address:* blair@slac.stanford.edu (B.N. Ratcliff).

angle resolution limit that depends on the detected photon bandwidth.

The number of photoelectrons observed ($N_{pe}$) is given by the Frank–Tamm equation

$$N_{pe} = 370 \, L \int \varepsilon \sin^2 \theta_c \, dE \qquad (2)$$

where $L$ is the length of the particle through the radiator in cm, $\varepsilon(E)$ is the overall collection efficiency for the Cherenkov photons multiplied by the detection efficiency for observing these photons as photoelectrons, and $E$ is the photon energy in eV.

Although it was first discussed in a classical paper by Tamm in 1939 [3], it seems to be less appreciated that the conical Cherenkov radiation shell is not perpendicular to the Cherenkov propagation angle in a dispersive medium. The half-angle of the cone opening ($\eta$) is given by

$$\cot \eta = [(n(\omega_0)\beta)^2 - 1]^{1/2} + \omega_0 n(\omega_0)\beta^2$$
$$\times (dn/d\omega)_0 [(n(\omega_0)\beta)^2 - 1]^{-1/2} \qquad (3)$$

where the index of refraction $n(\omega_0)$ is written as a function of the angular frequency ($\omega$) of the Cherenkov light with the frequency range centered at $\omega_0$. As Motz and Schiff pointed out in 1953 [4], the presence of the second term means that the cone angle ($\eta$) is the complement of the Cherenkov angle ($\theta_c$) only for a non-dispersive medium where $dn/d\omega = 0$.

After emission, the photon propagates a length $L_p$, in a time $t_p$

$$t_p = \frac{L_p n_g}{c} \qquad (4)$$

where the photon group velocity ($v_{group} = c/n_g$) must be used rather than the photon phase velocity ($v_{phase} = c/n$) since, in a dispersive medium, energy propagates at the photon group velocity. The relationship between group and phase velocities, as a function of photon wavelength $\lambda$, is usually derived in a simple 1D picture (see, e.g., Ref. [5]), and leads to the following relationship between the group and phase refractive indices:

$$n_g(\lambda) = n(\lambda) - \lambda \, dn(\lambda)/d\lambda. \qquad (5)$$

For fused silica, $n_g(\lambda)$ is typically several percent larger than $n(\lambda)$ for photons in the energy range

detectable by a bi-alkali photocathode. As a particular example, the weighted averaged value is $\langle n(\lambda)/n_g(\lambda) \rangle \sim 0.97$ for photons from a Cherenkov spectrum impinging on a bi-alkali photocathode after passing through a borosilicate window. More importantly for the resolution performance of a counter that uses timing, the dispersion of $n_g$ is also substantially greater, about a factor of 3 in the same photon energy range.

### 2.2. Cherenkov coordinate systems

For pedagogical purposes, it may be useful to write down specifically how the measured quantities are related to Cherenkov angles. Consider a frame (**q**), as shown in Fig. 1a, where the particle moves along the $z$-axis. The direction cosines of the Cherenkov photon emission in this frame ($\mathbf{q}_x$, $\mathbf{q}_y$, and $\mathbf{q}_z$), are related to the Cherenkov angles [see Eq. (1)] by

$$\mathbf{q}_x = \cos \varphi_c \sin \theta_c, \quad \mathbf{q}_y = \sin \varphi_c \sin \theta_c,$$
$$\mathbf{q}_z = \cos \theta_c \qquad (6)$$

and, defining the emission point ($z_e$) and detection point ($z_d$)

$$t_p = \frac{(z_e - z_d)n_g}{c\mathbf{q}_z}. \qquad (7)$$

Of course, photon coordinates are measured in some laboratory frame, such as that shown in Fig. 1b, and must therefore be transformed into the Cherenkov frame of the particle. Transforming between frames often makes use of externally derived tracking parameters. Though in principle this is straightforward, the transformation factors involved can be large and angle dependent. On the other hand, the individual photons from a given particle are strongly correlated (i.e., they all have the same Cherenkov polar angle), and the power of this ring correlation can be exploited either to reduce the required 'dimensionality' of each photon measurement or even to allow independent tracking of the particle trajectory.

As a specific example of several of these concepts in a rather complex system, consider the case of the DIRC shown schematically in Fig. 2. In the right-handed coordinate system attached to the indicated bar frame, we call the track polar and
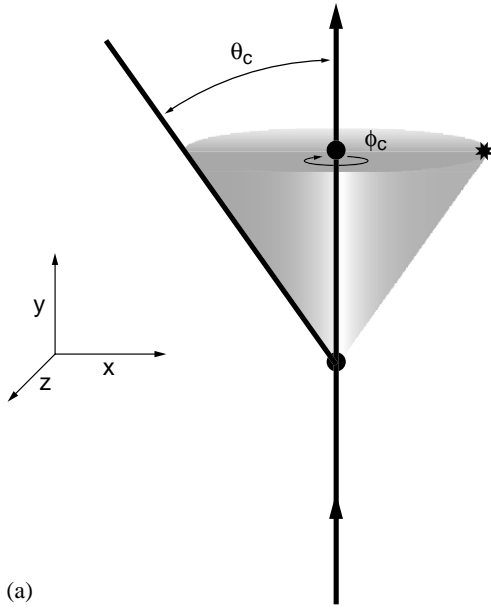
(a)
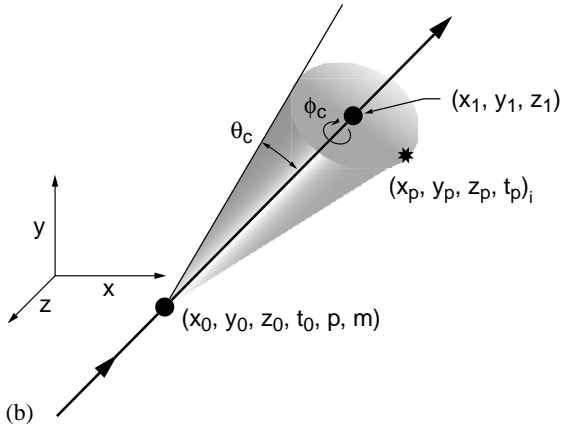


(b)

Fig. 1. Schematic of typical Cherenkov reference frames: (a) with respect to the particle path; and (b) in the lab coordinate system.

azimuthal angles $(\theta_t, \varphi_t)$. We align the **q** frame $x$-axis such that the direction cosines of the photon emission in the bar frame can be written as

$$k_x = -\mathbf{q}_x \cos \theta_t \cos \varphi_t + \mathbf{q}_y \sin \varphi_t + \mathbf{q}_z \sin \theta_t \cos \varphi_t,$$

$$k_y = -\mathbf{q}_x \cos \theta_t \sin \varphi_t - \mathbf{q}_y \cos \varphi_t$$
$$\qquad + \mathbf{q}_z \sin \theta_t \sin \varphi_t,$$

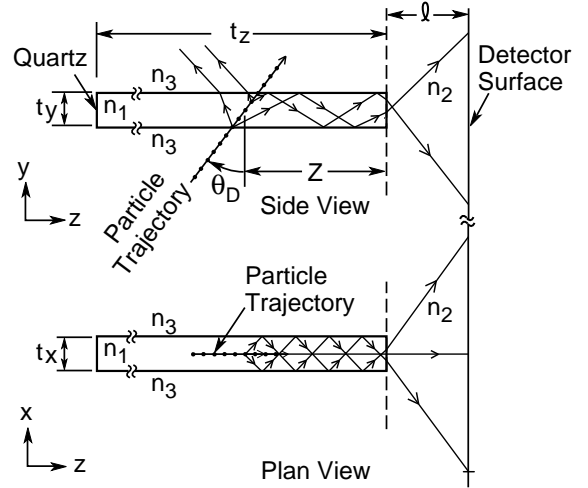$$k_z = \mathbf{q}_x \sin \theta_t + \mathbf{q}_z \cos \theta_t \qquad (8)$$



Fig. 2. Schematic of a radiator bar illustrating the DIRC reference frame. The particle trajectory is shown as a line connected by dots; representative trajectories of Cherenkov photons are shown by lines with arrows.

while the photon propagation time $t_p$ and propagation length $L_p$ down a bar length $L$ are given by

$$t_p = \frac{L_p n_g}{c} = \frac{L n_g}{c k_z}. \qquad (9)$$

DIRC is intrinsically a 3D imaging device. The three directly measurable quantities are typically a 3-space position of each 'hit' in a detector 'pixel' (e.g., a PMT), and its associated time. The space position provides a direct measurement of the two transverse angles with respect to the end of the bar $(\alpha_x, \alpha_y)$, assumed here to be corrected for refraction so that they are the angles inside the bar material. The third angle $(\alpha_z)$ can be calculated from the geometrical constraint. However, because of the long optical delay line, the photon propagation time down the bar ($t_p$, see Eq. (9)) is also directly related to the direction cosine of the photon angle along the bar $z$-axis (and thus to $\alpha_z$). This over-constraint is quite powerful in rejecting backgrounds and ambiguous solutions. It is usually only necessary to instrument one end of the bar and reflect photons heading the 'wrong' way back to the detector. The propagation time shift between the forward and backward going photons usually makes them easy to separate.

## 2.3. Performance limits

In a simple model, the fractional error on the particle velocity ($\delta_\beta$) is given by

$$\delta_\beta = \frac{\sigma_\beta}{\beta} = \tan\theta_c \sigma\theta_c$$

where

$$\sigma\theta_c = \frac{\langle \sigma[\theta_i] \rangle}{\sqrt{N_{pe}}} \oplus C. \tag{10}$$

$\langle \sigma[\theta_i] \rangle$ is the average single photoelectron resolution, and $C$ is a correlated component combining contributions from several sources including tracking and alignment errors and multiple scattering. Clearly, for the best resolution, it is best to maximize $N_{pe}$ while minimizing $C$ and $\langle \sigma[\theta_i] \rangle$. However, for any given photon detection efficiency curve, in a fixed radiator length counter, the only way to increase $N_{pe}$ is to increase the photon detection bandwidth ($\Delta\lambda$) which also increases the chromaticity contribution to $\langle \sigma[\theta_i] \rangle$ so there is an 'intrinsic' chromaticity performance limit to attainable performance. In practice, there are many other 'practical' limits due to photon detector availability and performance, geometrical and radiator length considerations, attainable radiator size, and production specifications, and costs. For a $\beta \approx 1$ particle of momentum $p$ well above threshold entering a radiator with index of refraction $n$, the number of $\sigma$ separation $N_\sigma$ between particles of mass $m_1$ and $m_2$ is approximately

$$N_\sigma \approx \frac{|m_1^2 - m_2^2|}{2p^2 \sigma[\theta_c(tot)]\sqrt{n^2 - 1}}. \tag{11}$$

In practical counters, the attainable angular resolution term $\sigma[\theta_c(tot)]$ varies between about 0.5 and 5 mrad depending on the size and radiator type of the particular counter. The momentum coverage range of a particular counter is largely determined by the radiator index. Low indices are required to cover high momenta, but the radiators must become very large to produce sufficient photons.

## 3. Imaging methods

### 3.1. Introduction

The following sections provide a brief, schematic review of imaging methods that can be used in RICH detectors. Though the DIRC is a sub-type of RICH, the presence of the light guides with long path lengths leads to somewhat different considerations, particularly for the timing dimension, than for more classical RICH designs; Thus for clarity, DIRC and RICH examples of the relevant methods will both be given. Unless it is essential for clarity, complications such as different refractive indices in the imaging and radiator regions are ignored. Imaging can be thought of as occurring in each of the three possible dimensions (two space and one time), and different imaging methods can be chosen in each dimension if desired. As the speed of light is so fast, precision imaging in the time dimension is practical only when the photon propagation paths are long (e.g., in DIRCs or large water Cherenkov counters).

### 3.2. Proximity

The classic 'proximity' focusing scheme, typically used for liquid/solid radiator RICH counters, is shown in Fig. 3. In this scheme, the photon's angles are measured by comparing its detected position with respect to its emission point along the track. This requires knowledge of the position of the input track and the path of the photon to the detector. A simple estimate of the angular resolution on the measured angle $\alpha$ for
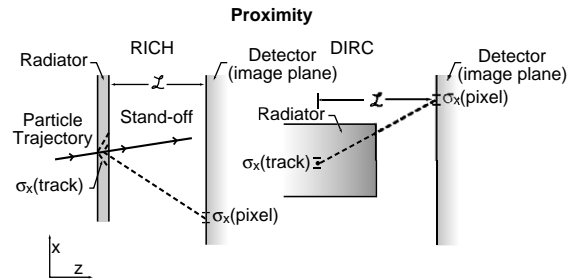


Fig. 3. Proximity imaging scheme.

this method is

$$\sigma_\alpha \approx \sqrt{\frac{\sigma_x^2(\text{track}) + \sigma_x^2(\text{detector})}{L^2}}. \tag{12}$$

For a RICH of the SLD/DELPHI [6] type with [$\sigma_x(\text{track}) \sim 2\,\text{mm}$, $\sigma_x$ (detector) $\sim 1\,\text{mm}$, and $L \sim 200\,\text{mm}$], $\sigma_\alpha \sim 11\,\text{mrad/photon}$. For a DIRC, the relevant 'standoff' length ($L$) is the distance from the track to the detector which may be quite long. For example, a DIRC like that of BaBar [7] with [$\sigma_x$ (track) $\sim 4\,\text{mm}$, $\sigma_x(\text{detector}) \sim 6\,\text{mm}$, and $L \sim 4000\,\text{mm}$], $\sigma_\alpha \sim 2\,\text{mrad/photon}$. The price paid for this excellent resolution is that the bar bounce ambiguities must be resolved. Excellent time resolution can help.

### 3.3. Pinhole

The 'Proximity' focusing scheme discussed above is related to, yet subtly different than, the 'pinhole' focusing method used by the BaBar DIRC, shown in Fig. 4. This later imaging scheme is a direct analog of the pinhole camera, hence the name, but has no simple analog in classical RICH counters. In this method, the path of the photon down the DIRC bar is ignored, and the resolution is independent of the precise track location in the bar. It does, however, depend directly on the size of the bar exit aperture $t_x$

$$\sigma_\alpha \approx \sqrt{\frac{t_x^2/12 + \sigma_x^2(\text{detector})}{L^2}}. \tag{13}$$

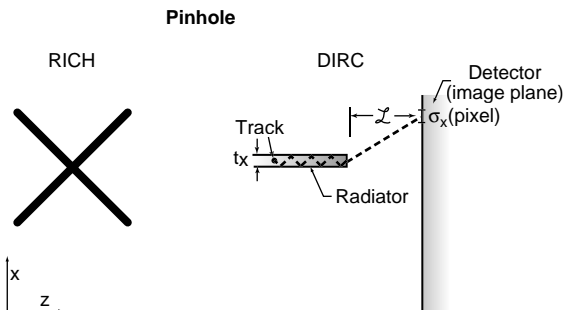The relevant standoff length becomes the distance from the bar end to the detector plane, rather than the distance from the track to the detector plane. This is normally shorter than for the 'proximity' focused scheme of Section 3.2. However, the multiple bar bounce ambiguities no longer need to be resolved. For example, for the BaBar DIRC with [$t_x(t_y) \sim 35(17.5)\,\text{mm}$, $\sigma_x$ or $\sigma_y \sim 7.5\,\text{mm}$, and $L \sim 1200\,\text{mm}$], $\sigma(\alpha_x(\alpha_y)) \sim 10.5(7.5)\,\text{mrad}$ per photon if the standoff region were made from fused silica. Since this region is actually filled with water in the BaBar DIRC, the resolution is about 10% better than this estimate due to magnification at the interface.

### 3.4. Lens

Fig. 5 shows one version (a single reflective lens) of 'lens' focusing. Other versions of lens focusing could use refractive, gradient, or diffractive lens, but the reflective system has the advantage for DIRC that it allows the same material in the focusing region as in the bars thus maximizing the overall efficiency for photon propagation. The advantage of a focusing scheme of this kind, compared to the pinhole scheme, is that the bar size can, in principle, be removed from the resolution equation and excellent resolution can be attained if the number of pixels is sufficiently large. One can also magnify or de-magnify the image to match the pixel size of a particular detector device.

Neglecting aberrations, the angular resolution is given by

$$\sigma_\alpha \approx \sqrt{\frac{\sigma_x^2(\text{detector})}{L^2}}. \tag{14}$$
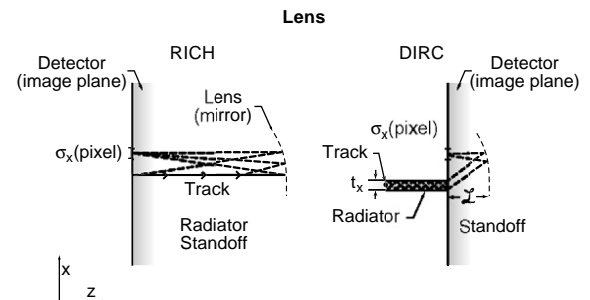


Fig. 4. Pinhole imaging scheme.



Fig. 5. Lens imaging scheme.

For example, for a $\sigma_x(\text{detector}) = 0.6$ mm (equivalent to a detector with 2 mm pixels) and $L = 250$ mm, $\sigma(\alpha_x) \sim 2.4$ mrad per photon.

### 3.5. Time

Fig. 6 illustrates the principle of imaging in the timing dimension. In 'classical' gaseous photocathode RICH counters, the distances are too short and/or time of propagation known too poorly for this method to be viable. The use of timing in very large water Cherenkov counter is discussed in the next section. For DIRC, Eq. (9) shows that the direction cosine along the $z$-axis ($k_z$) is inversely related to the photon propagation time, so that in the non-dispersive limit

$$\sigma_{\alpha_Z} \approx \frac{c \cos^2 \alpha_Z \sigma_t}{N_g L \sin \alpha_Z}. \tag{15}$$

and one might naively conclude that the resolution on the photon dip angle is inversely related to the distance the photon travels down the bar. Of course, it also depends on the dip angle. However, the dispersive component of the group refractive index is large enough to become a dominant component in many real-world cases so that the resolution quickly reaches the dispersive limit

$$\sigma_{\alpha_z} \approx \frac{\delta n_g}{\tan \alpha_z}. \tag{16}$$

The fractional resolution on $n_g$ [$\delta(n_g) = \sigma(n_g)/n_g$] is about 0.015 for bi-alkali tubes, averaged over the Cherenkov emission spectrum. So, if the time resolution per photon is assumed to be so small that the dispersion dominates the

resolution of the photon 'dip' angle $\alpha_z$, the error $\sigma_{\alpha_Z} \sim 0.015/\tan \alpha_z$ varies from a practical minimum of about 9 mrad for large transverse photon propagation angles ($\alpha_z \sim 60°$) in the bar to an infinite maximum at $\alpha_z = 0°$, where the photon travels along the bar axis. For a typical $\alpha_z$ of $\sim 30°$, the angular error from dispersion alone is $\sim 25$ mrad.

### 3.6. Ring correlated

Full tracking (and event) reconstruction is performed with a fitting optimization procedure in large water Cherenkov counters (see, e.g., Ref. [8]) by combining the space position and time of each photon together with the constraint that the individual Cherenkov photons are emitted from each track at a constant polar angle (see Fig. 1b). As these devices are very large, the propagation distances and times for individual photons are correspondingly large. Thus, reasonable tracking precision can be attained even with rather modest space point and time resolution on each photon. The individual tracks can be tied together in an event, and tracking and event parameters such as vertex position, number of tracks, track momenta, number of Cherenkov photons per track, and the particle type (as e or muon using the ring width) can be determined. Though individual tracks are generally not determined solely in this way in the PID type detectors used in most HEP accelerator experiments, fit optimization using the ring correlation is still often done to improve the parameters of the track as it passes through the radiator, and thus to reduce the correlated component of the Cherenkov angular determination.

### 3.7. Some examples

It may be helpful to list a few examples of some counters that use the imaging principles discussed above. Proximity imaging is used by CLEO-III [9], and the DELPHI-RICH and SLD-CRID liquid radiators [6]. Pinhole imaging is used by BaBar-DIRC [7], while lens imaging has been used in many different devices including the gas radiators for DELPHI-RICH and SLD-CRID [6]; OMEGA RICH [10]; gas and aerogel radiators in HERMES
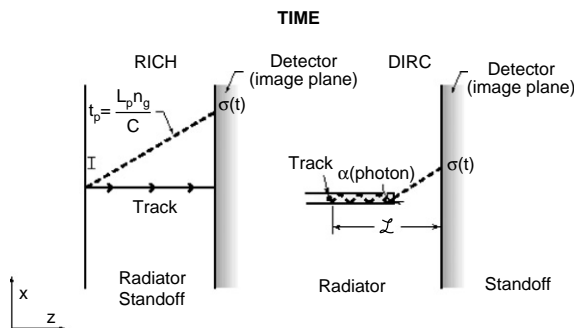


Fig. 6. Time imaging scheme.

[11]; and HERA-B RICH gas [12]. Time imaging has been used in the BaBar DIRC [7] and several R&D devices [13,21] (see Section 4.3). Correlated imaging is a staple feature of the large water or ice Cherenkov counters such as Super-Kamiokande [8] and AMANDA [13].

## 4. Time imaging in DIRCS

### 4.1. Conceptual issues

We now turn to a more detailed look at some specific issues associated with time-dimension imaging in DIRCs. As discussed earlier, the chromatic dispersion that is relevant to the variation in the produced Cherenkov angle is the index of refraction dispersion $\delta n = \sigma(n)/n$, so that for the 'ith' photon with track $\beta = 1$

$$\sigma_{\theta_c}(i) = \frac{\delta n}{\tan \theta_c}. \tag{17}$$

For a typical bi-alkali PMT (e.g., the BaBar DIRC EMI 9125 with a fused silica radiator), $\sigma(\theta_c(i)) \sim 4.9$ mrad. On the other hand, the fractional chromatic time dispersion during photon propagation ($t_p$) is controlled by the value and dispersion of the group index ($n_g$), the propagation length ($L_p$), and a correlated term $C$, so that

$$\delta^2[t_p(i)] = \delta^2[L_p(i)] + \frac{2C(L_p, n_g)}{L_p(i) n_g(i)} + \delta^2[n_g(i)]. \tag{18}$$

The correlated term depends on the photon dip angle, and its measurement accuracy. For simplicity, in fused silica it is useful to write the resolution in the form

$$\delta^2[t_p(i)] = F \times \delta[n_g(i)] \approx 0.016 \times F \tag{19}$$

where $F$ depends on the photon dip angle and its measurement accuracy. Typically, $F$ ranges between about $\frac{2}{3}$ and $\frac{4}{3}$ and is smallest for large photon dip angles (i.e., for those that bounce many times in the bar).

With an intrinsic photon detector chain resolution of ($\sigma(t_0)$), the measured time resolution ($\sigma(t_m)$) for each photon is

$$\sigma^2(t_m) = \sigma^2(t_0) + t_p^2 \delta^2(t_p). \tag{}$$
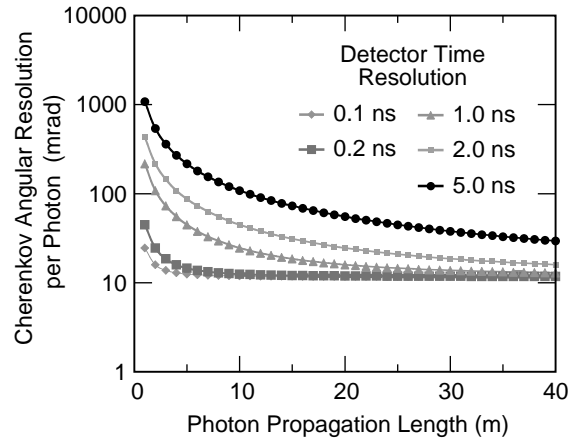


Fig. 7. Cherenkov polar angular resolution versus photon propagation length for several values of detector time resolution.

The most favorable track dip angle for using timing to measure the Cherenkov angle is near 0 degrees (i.e, for $(\theta_t, \phi_t) = (90°, 90°)$) where

$$\sigma(\theta_c) = \tan \theta_c (\mathrm{sqrt}[\delta^2(n_g) + 2C(n_g, t_p)\delta(n_g) \\ \times \delta(t_p) + \delta^2(t_p)]). \tag{20}$$

Fig. 7 shows the Cherenkov polar angle resolution attainable in this case, for a bi-alkali type response detection curve with a fused silica radiator as a function of detector time resolution and photon propagation length. The resolution attainable saturates at about 10 mrad per photon independent of detector timing performance. However, this saturation in performance is attained at 2–3 m in length if the detector resolution is $\sim 100$ ps, while the propagation length must grow longer to reach saturated performance as the resolution gets worse.

As already discussed, at other angles the performance is less favorable, both because of the geometrical effect from the dip angle and because the negative correlation between production angle and propagation time becomes smaller, or in the least favorable cases, becomes positive.

### 4.2. Limits to single photon performance

It is interesting to consider how the measurement errors might be reduced. The total error on

the Cherenkov polar angle scales as shown by Eq. (10)

$$\sigma_{\theta_c} = \frac{\langle \sigma[\theta_i] \rangle}{\sqrt{N_{pe}}} \oplus C. \qquad (21)$$

The error on each individual photon $\sigma[\theta_i]$ can be thought of as being given in terms of a number of individual design components

$$\sigma[\theta_i]$$
$$= \sqrt{\sigma[\theta_{Pr}]^2 + \sigma[\theta_{Tr}]^2 + (\sigma[\theta_{Im}]^2 + \sigma[\theta_{De}]^2)}. \qquad (22)$$

The Imaging and Detection terms, defined as ($\sigma[\theta_{Im}]$, $\sigma[\theta_{De}]$), have been discussed together in Section 3. In principle, angular resolution derived from positional information can be made 'arbitrarily' good to match requirements for a particular performance limit. In particular, the imaging component that comes from the bar size in a pin hole focusing scheme, such as the one used by BaBar, can be made small with lens focusing, and the number of detector pixels and the standoff distance are essentially arbitrary choices. It makes economic sense to choose focusing methods and detector configurations that balance the various resolution components.

Transport smearing, defined as ($\sigma[\theta_{Tr}]$), can be caused by various flaws in the DIRC radiators, such as non-parallel sides, non-planar surfaces, and non-orthogonal sides and faces. In general, photons at small dip angles in the bar tend to be most distorted. These also tend to be lost due to index matching problems between radiators, glues, and imaging-region materials. Due to effects of these kinds, the resolution contribution from this term tends to grow as the square root of the propagation length and becomes worse than expected for the large transverse angle photons. In BaBar DIRC, the most difficult effect of this kind to control was the side-to-face orthogonality, which contributes around 2–4 mrad per photon for a bar at the production specification limit. In principle, such effects can be made much smaller with different production methodology (at a higher cost), or by using a 1D transport design to limit the number of side bounces. BaBar DIRC also retains few photons with dip angles less than

about 30° because of the water-fused silica interface.

The dominant smearing term at production, defined as ($\sigma[\theta_{Pr}]$), is the so-called production chromatic term ($\sigma[\theta_{Chromatic}]$) discussed earlier. Other production smearing terms, such as trajectory distortion due to bending in the magnetic field, or multiple scattering in the radiator material, are much smaller at least at high momentum where good resolution is required to separate πs from Ks.

### 4.2.1. Mitigating chromatic smearing

It seems impractical to apply chromatic correction in the focusing system, or to find a radiator with significantly less dispersion than fused silica. However, somewhat counter-intuitively, limiting the detector acceptance bandwidth can actually improve the total resolution substantially in a DIRC with resolution near the chromatic limit even though such a restriction limits $N_{pe}$ substantially. Of course, this ignores the pattern recognition issues. Nonetheless, e.g., the total contribution $\sigma[\theta_c(tot)]$ from the chromatic term in a counter with a glass window bi-alkali detector response is reduced by a factor of about 2.5 when the photon energy range is restricted between 600 and 450 nm compared to the case where all photons between 600 and 300 nm are accepted, even though the number of photons observed is reduced by nearly a factor of four! If a high-efficiency detector were available in a longer wavelength region near the visible, this could lead to excellent performance for a counter operating near the dispersion limit.

The 'ideal' solution to the chromatic smearing would be a detector that measures the photon energy directly. In principle, some detectors of this kind exist (e.g., the transition edge sensors [14]), but they are slow, run at 70 mK, and would be very hard to implement. It seems more practical to use the large dispersion of $n_g$, as described earlier, to measure the photon wavelength directly in a 3D DIRC. That is, by comparing the individual photon flight time with its measured angle, the photon wavelength can be calculated. This allows the refractive index at production to be rather precisely calculated so that the chromatic

piece of the production term can be substantially reduced. The measurement of photon wavelength done in this way can be quite accurate if the time resolution is good ($\sim$100 ps). In the Cherenkov angle space, for a long DIRC this would be equivalent to reducing the smearing due to chromaticity by a factor of about 5 (to about 1 mrad per photon). The large chromatic dispersion of the group velocity actually works in one's favor in this case!

### 4.2.2. Mitigating other resolution terms

There are also a number of additional limits to particle separation performance that should be mentioned. The first are the correlated terms. These can come from many sources, including multiple scattering, alignment systematics, tracking performance, etc. Because these contribute to the total resolution on the angle, they must be held well under 1 mrad in order to obtain significantly improved performance. The second come from physics processes, such as decay, interactions, δ-rays, etc. In principle, many of these terms could be addressed, at least in part, with a high-precision post-PID-tracking device.

### 4.3. R&D examples

Although no high-precision timing DIRC for particle ID has yet been used in an experiment, a number of interesting R&D devices that use precision timing have been constructed and some properties explored in R&D devices. Two such devices with 1D or 2D readout (the 1D CCT and the 2D TOP) have already been discussed briefly above. Since they have been described in detail at either this conference (the TOP [15]) or earlier meetings in this conference series (the CCT [16,21]), in the interest of brevity, they will not be further discussed here. Please refer the references for a complete description. For comparison, we will briefly explore some features of two full 3D devices that have been proposed by the BaBar DIRC group during the past decade, as they have not been discussed in any detail at this series of meetings.
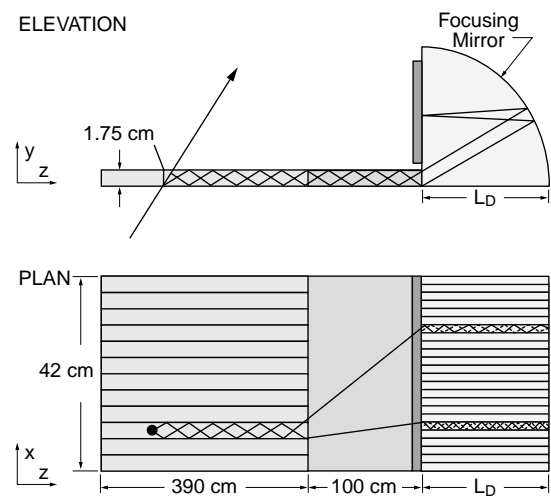


Fig. 8. BaBar DIRC conceptual Design II with pixilated readout.

### 4.3.1. BaBar DIRC conceptual design (II)

During the design phase of BaBar, Hamamatsu began to deliver pixilated Metal Channel Dynode tubes in the R5900 series. This led to an alternative design for BaBar DIRC (see, e.g., Ref. [17]) as shown in Fig. 8.

This is a full 3D design: 1D pinhole ($x$) with a 100 cm standoff, 1D lens ($y$), and fast timing. It is modular, compact, and was thought to be easier to engineer than the conventional, water-filled imaging-region device as it has no potential for water leaks. The fast timing provides some help on angular resolution and is very effective in sorting out the ambiguities. This device is also very resistant to all backgrounds, because of its speed, and since it is much more compact, it would be less sensitive to random backgrounds in the imaging region than the device with a water-filled region. However, when it was proposed, it still required further development of the Hamamatsu 5900 series tube technology to get a 64 channel, linear array tube with better geometrical coverage than existing models. Though the manufacturer was willing to work on developing such a tube, there were many unknowns about tube uniformity, quantum efficiency, cross talk, active area ratio, etc. If all of these issues could be solved, nominal separation performance in simulations was predicted to be fairly similar to (or a bit better) than

that of the water standoff device actually built. However, as so little was known (or knowable) about the actual detector performance at the time a decision was required there was too much technical risk to head down an untrodden road with no fallback possible.

### 4.3.2. Super BaBar

Super BaBar is a concept for a detector capable of doing physics at a very high luminosity (Lum = $10^{36}$) e + e− Super-PEP collider operating at the Y(4S) [18]. This would be a totally new machine, not an approved upgrade of the existing PEP-II machine. The first concern for a PID system operating at such a machine would be to at least maintain the existing BaBar separation performance. To do this, it is necessary to cope with the very high backgrounds expected at such a machine. Some of the important tools available to fight backgrounds are (1) fast timing; (2) 3D imaging; and (3) careful shielding of beams. All are likely to be required. In addition, if at all possible, it would be very useful to improve the overall separation performance, both by improving the angular resolution (and the momentum range of coverage), and by improving the mis-id rates and the correlated terms.

The design tools available have been discussed above. A concept for a detector that meets these requirements is given in Fig. 9. The design details will depend on the photon detector, but as an example, if the detector has 120 pixels in the $y$ direction, $\sim 1$–2 cm pixels in $x$, and $<150$ ps resolution in time, $\pi/K$ should be separable by more than $3\sigma$ to above 6 GeV/c. Post PID tracking should be incorporated as it would allow significant reduction in correlated and physics-dependent terms, such as alignment, tracking and decay systematics, leading to better mis-id rates.

There are, of course, many practical details involved in constructing such a device. For example, one must demonstrate that the ambiguities and backgrounds can be handled and that the large radiator pieces can be constructed to the required specifications. However, the availability of photodetectors with the needed properties continues to be 'the' crucial element for design, and the R&D of the BaBar group is centered
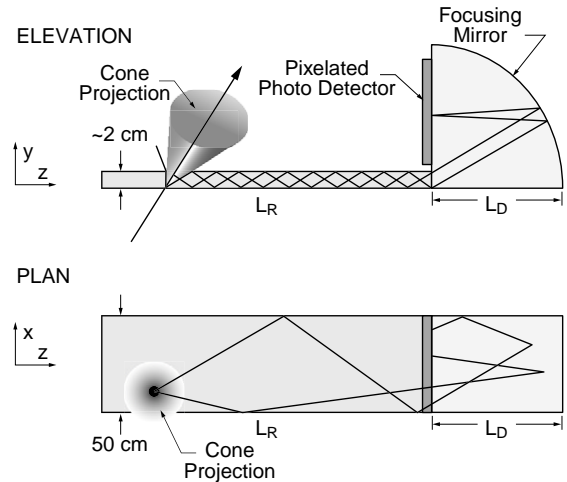


Fig. 9. A 3D DIRC conceptual Design for Super BaBar.

primarily on this issue at the present time. The newest flat panel PMTs by Hamamatsu [19] are now becoming available and may provide an adequate solution. Hybrid PMTs could also be a promising alternative for the future [20], but they are probably too slow. Other potential technologies, such as Hybrid Avalanche Photodiodes, visible light gas detectors, and MCP-PMTs have many attractive features but remain more speculative at present. Finally, the affordability of the 25–40 K channels of readout needed will clearly be a challenge.

## 5. Summary

Tom Ypsilantis was seminal to the evolution of RICH counters from an early concept into the powerful instruments now in place and also to this enlightening series of RICH conferences. He was truly the 'Lord of the Rings'. Unlike the Lord from Mordor who has darkened the world of the movie screen, Tom brought light, joy, and keen understanding to the detector world, not only with his powerful independent efforts but also in supporting the efforts of his many friends. The author still finds it difficult to believe he is not here with us. With grateful thanks to our Lord of light, Tom, and apologies to J.R.R. Tolkien:

**The Lord of the Rings**

Photons from ice and sea under the sky,
  Photons from vast water tanks in halls of stone,
Photons from the atmosphere in an insect's eye,
  Photons from aerogels, light, clear, blown,
Photons from liquids, gases, crystals flying by,
  Photons from fused silica expanding on a cone.
In RICH detectors where PID truths lie.
  One Ring to rule them all, One Ring to find them,
  One Ring to bring them all, correlate, and bind them
In RICH detectors where PID truths lie.

**References**

[1] B.N. Ratcliff, S. Spanier, Nucl. Instr. and Meth. A 433 (1999) 456.
[2] B.N. Ratcliff, SLAC-PUB-8989 and ICFA Instrum. Bull. 22:03, 2001.
[3] I. Tamm, J. Phys. USSR 1 (1939) 439.
[4] H. Motz, L.I. Schiff, Am. J. Phys. 21 (1953) 258.
[5] J.D. Jackson, Classical Electrodynamics, 4th Edition, 1965, p. 211.
[6] E. Albrecht, et al., Nucl. Instr. and Meth. A 433 (1999) 47; J. Va'vra, Nucl. Instr. and Meth. A 433 (1999) 59.
[7] J. Schwiening, et al., Presentation at this conference (RICH2002).
[8] M. Shiozawa, Nucl. Instr. and Meth. A 433 (1999) 240.
[9] S. Stone, Presentation at this conference (RICH2002).
[10] U. Muller, et al., Nucl. Instr. and Meth. A 433 (1999) 71.
[11] H. Jackson, Presentation at this conference (RICH2002).
[12] S. Korpar, Presentation at this conference (RICH2002).
[13] A. Hallgren, Presentation at this conference (RICH2002).
[14] B. Cabrera, et al., Appl. Phys. Lett. 73 (1998) 735.
[15] T. Ohshima, Nucl. Instr. and Meth. A 453 (2000) 331, and presentation at this conference (RICH2002).
[16] Kichimi, et al., Nucl. Instr. and Meth. A 371 (1994) 306.
[17] G. Lynch, B. Ratcliff, J. Veillet, private communication.
[18] SLAC-PUB-8970, 2001.
[19] Hamamatsu Photonics K.K., http://www.hamamatsu.com/.
[20] A. Braem, et al., Nucl. Instr. and Meth. A 433 (1999) 153.
[21] K. Honscheid, M. Selen, M. Sivertz, Nucl. Instr. and Meth. A 343 (1994) 306.